Rectangular Jets in a Crossflow

M. S. Kavsaoglu,* J. A. Schetz,† and A. K. Jakubowski‡
Virginia Polytechnic Institute and State University, Blacksburg, Virginia

Rectangular jets injected from a flat plate into a crossflow at large angles have been studied. Results were obtained as surface pressure distributions, mean velocity vector plots, turbulence intensities, and Reynolds stresses in the jet plume. The length-to-width ratio of the jets was 4, and the jets were aligned streamwise as single and side-by-side dual jets. The jet injection angles were 90 and 60 deg. Surface pressure distribution results were obtained for jet-to-freestream velocity ratios of 2.2, 4, and 8. Mean flow and turbulence flowfield data were obtained for the side-by-side dual jets, mainly for the jet-to-freestream velocity ratio of 4. The jets featured strong negative pressure peaks near the front nozzle corners. The 60-deg jets produced lower magnitude negative pressures, which are distributed over a lesser area when compared to the 90-deg jets.

Nomemclature

A	= area
C_p	= pressure coefficient
ΔC_p	= $C_{p_{\text{jet on}}} - C_{p_{\text{jet off}}}$
D_{ref}	= diameter of a same area circle
L	= length
p	= static pressure
q	= dynamic pressure
R	= jet-to-freestream velocity ratio
S	= center-to-center spacing
U, V, W	= velocity components
U_{TOT}	= $\sqrt{U^2 + V^2 + W^2}$
u', v', w'	= fluctuating velocity components
$\tilde{u}, \tilde{v}, \tilde{w}$	= $\sqrt{\overline{u'^2}}/U_{\text{TOT}}$, $\sqrt{\overline{v'^2}}/U_{\text{TOT}}$, $\sqrt{\overline{w'^2}}/U_{\text{TOT}}$
$-\widetilde{uv}$, $-\widetilde{uw}$, $-\widetilde{vw}$,	= $-\overline{uv}/U_{\text{TOT}}^2$, $-\overline{uw}/U_{\text{TOT}}^2$, $-\overline{vw}/U_{\text{TOT}}^2$

Subscripts

j	= jet
∞	= freestream
T,TOT	= total
S	= static

Introduction

CROSSFLOW jet injection has a large area of application, which includes industrial chimneys, sewage outfalls, fuel injection into combustion chambers, film cooling, and the transition flight of the VTOL aircraft. The present work is a fundamental research study aimed primarily toward the application to VTOL aircraft, although the results have broader utility. This flow problem can be idealized as crossflow jet injection from a slender body of revolution or from a flat plate. Crossflow jet injection from a surface produces negative pressures on the surface, particularly toward the downstream and to the sides of the jet exit. There will also be a positive pressure region due to crossflow deceleration. Negative pressures on the bottom surface of a wing means loss of lift for an aircraft. When these negative pressures combine with the positive pressure region in front of the jet, the resultant effect is to produce a nose-up pitching moment. This pressure distribution is strongly dependent on the jet-to-freestream velocity ratio, which is continuously changing during the transition flight.

The number of parameters involved in the general problem of jets in a crossflow is large: jet-to-freestream velocity ratio, jet exit geometry (circular, rectangular, etc.), jet injection angle, single jet or side-by-side or tandem multiple jets, jet exit velocity profile (uniform, nonuniform, swirling, etc.), jet exit turbulence levels, temperature difference between jet and freestream, concentration profiles, two-phase flows, and buoyancy effects, to name some. If one or both of the streams is supersonic, additional parameters would be involved. The present work deals with low-speed, gaseous rectangular jets. Available experimental information on rectangular jets is very limited when compared to circular jets. Streamwise aligned rectangular jets might have some practical advantages over the circular ones for VTOL aircraft. For example, they can be placed to the sides of an aircraft more easily, and they make less blockage against the crossflow for the same jet exit area.

A list of selected publications and research papers related to crossflow jet injection is given here as Ref. 1-23. A larger list can be found in Ref. 22. General information on crossflow jet injection can be obtained from Ref. 1. Reviews of the previous works can be found in Refs. 3-5. Information on previous works in a tabulated form can be found in Refs. 11 and 23 (or Ref. 22). Previous researchers have usually presented their results as surface pressure distributions, jet trajectories, and/or mean velocity vector plots. Sparse temperature field and turbulence information are also available.

According to previous researchers, some of the important characteristics of these types of flows are known. A pair of counter-rotating vortices is formed by the interaction of the jet and the crossflow. These vortices are deflected downstream and lie on the concave side of the jet centerline.[14] Air from the freestream is accelerated in the direction of the jet by viscous entrainment of surrounding fluid. A low-pressure region is created on the plate surface. This effect becomes more pronounced as the velocity ratio increases.[14] The boundary of the jet acts like a solid cylindrical body placed in the crossflow. This blockage effect causes the flow to separate as it travels around the jet, and a low-pressure wake region forms near the surface.[14] This background can be used to help interpret the new results here.

The present work is most closely related to Refs. 6-10. In Ref. 6, single and tandem dual circular jets injected from a body of revolution were investigated. In Ref. 7, side-by-side

Presented as Paper 86-0477 at the AIAA 24th Aerospace Sciences Meeting, Reno, NV, Jan. 6-9, 1986; received Jan. 20, 1986; revision received Oct. 19, 1987.

*Graduate Research Assistant, Aerospace and Ocean Engineering Department; currently at Middle East Technical University, Department of Aeronautical Engineering, Ankara, Turkey.

†W. Martin Johnson Professor and Department Head, Aerospace and Ocean Engineering Department. Fellow AIAA.

‡Associate Professor, Aerospace and Ocean Engineering Department. Member AIAA.

Table 1 Scope of the present research[a]

Jet type	Jet velocity profile	Jet velocity, m/s	$U_j/U_{\infty=R}$ Pressure data	$U_j/U_{\infty=R}$ Mean flow data	$U_j/U_{\infty=R}$ Turbulence data
90-deg single rectangular	Uniform nozzle	66	2.2, 4, 8	—	—
90-deg side-by-side dual rectangular	Uniform nozzle	66	2.2, 4, 8	2.2, 4	4
60-deg single rectangular	Uniform nozzle	66	2.2, 4, 8	—	—
60-deg side-by-side dual rectangular	Uniform nozzle	66	2.2, 4, 8	4	4

[a]For rectangular jets: $L = 86$ mm, $W = 21.5$ mm, $L/W = 4$, and jet aligned streamwise. For side-by-side dual rectangular jets: $S/D_{ref} = 0.95$ (D_{ref}: D of same area circle).

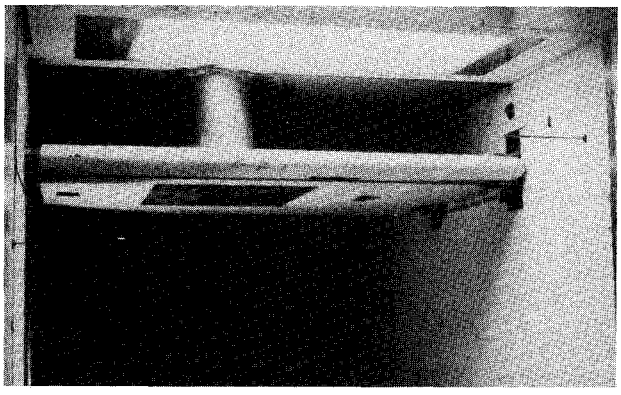

a) View looking downstream

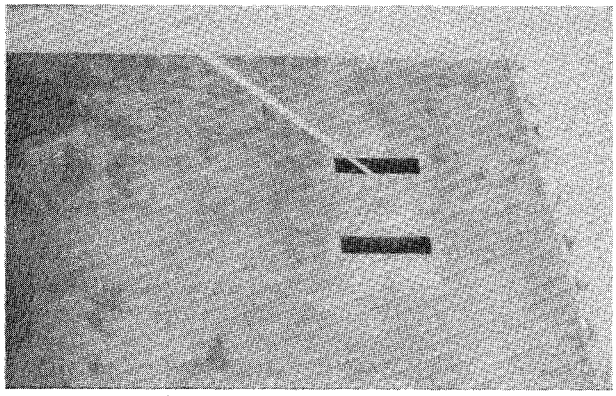

b) View of the instrumented section

Fig. 1 Photographs of the model in the wind tunnel.

and tandem dual circular jets injected into crossflow from a flat plate were considered. In Ref. 8, the effects of nonuniform velocity profiles on crossflow jet injection from a flat plate have been studied. In Ref. 9, single and side-by-side dual rectangular jets injected at a 90-deg angle were studied. Those test were repeated during the course of the present research. The difference between the jets of Ref. 9 and the present work is that those jets were found to have had some rotation in their center, but the jets of the present work had quite uniform exit profiles. Reference 18 is an example of earlier experimental studies related to rectangular jets. In that reference, a single rectangular jet with an aspect ratio of 4 was studied. The jet was aligned across and streamwise. References 11, 12, 20, and 21 are examples of the limited turbulence measurements available in the plume of crossflow jets.

The test matrix for the present research can be seen in Table 1. Both 90 and 60-deg single and side-by-side dual rectangular jets were studied. The jets were aligned streamwise and had sharp corners. For the 90-deg case, the rectangular jet length-to-width ratio (L/W) was 4. For side-by-side 90-deg rectangular jets, the ratio of jet spacing to reference diameter (S/D_{ref}) was 0.95. The jet exit areas were equal to the jet exit areas of Refs. 6–8 and 10 for a 90-deg circular jet. The 60-deg jets had the same shape and dimensions as the 90-deg ones when cut with a plane perpendicular to the jet axis. These quantities were selected as representative of the VTOL cases. The rectangular jets had uniform velocity profiles and low exit turbulence (approximately 3%). The jets were injected from a flat plate that was large compared to the jet/crossflow interaction area. Results were obtained as surface pressure distributions, mean velocity vector plots, turbulence intensities, and Reynolds stresses. Surface pressure distribution tests were done for jet-to-freestream velocity ratios of 2.2, 4, and 8. These tests were done for single and dual jets. Mean velocity vector plots were obtained for dual jets and for $R = 2.2$ and 4 for the 90-deg case and $R = 4$ for the 60-deg case. Turbulence intensities in the jet plume were obtained for $R = 4$ for 90 and 60-deg dual jets. More detailed information about the present research can be obtained from Ref. 22.

Apparatus

Wind Tunnel and Data Acquisition

The experiments were carried out in the 6×6-ft (1.83×1.83-m) Stability Tunnel at Virginia Tech.[24] The tunnel has a very low turbulence flow. Tunnel speeds in the range of 24 to 102 ft/s (8.52 to 31.04 m/s) were used according to need.

Test Model

The flat-plate model is shown in Figs. 1 and 2. It is mounted 45.7 cm (18 in.) below the top of the test section with the jets exhausting downward. The model has a rounded leading edge and a tapered trailing edge. A 5.08-cm (2 s in.) wide strip of sandpaper was glued to the plate 11.4 cm (4.5 in.) back from the leading edge to keep the boundary-layer turbulent at low tunnel velocities. Each nozzle is located in a 10.16-cm (4.0 in.) removable brass square section and has an exit area of 2.16×8.57-cm (90-deg jets). The spacing between the center lines of the nozzles is 10.16 cm (4.0 in.).

An area of 40.64×40.64-cm (16×16-in.) around the nozzles is instrumented with pressure taps. The pressure taps were located with a 0.64-cm (0.25 in.) spacing in nozzle sections and a 1.7-cm (0.67 in.) spacing in other locations. After ignoring a few damaged ports, more than 900 ports were used for data processing, and more than 400 of these ports were in the nozzle section.

Jet Nozzles

Figure 2b shows the layout of the nozzles. Each jet is produced by means of an electric blower. Air coming from each blower follows a circular pipe of 8.6-cm (3.38 in.) diam. It passes through a circular-to-square adaptor section, and then it runs into a 8.57×8.57-cm-square channel of length 25 cm.

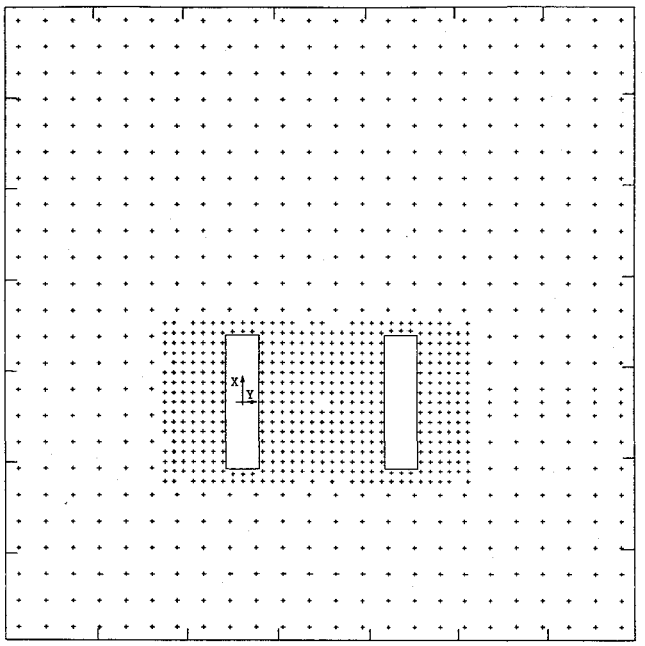

a) Pressure tap locations for 90 deg rectangular jets

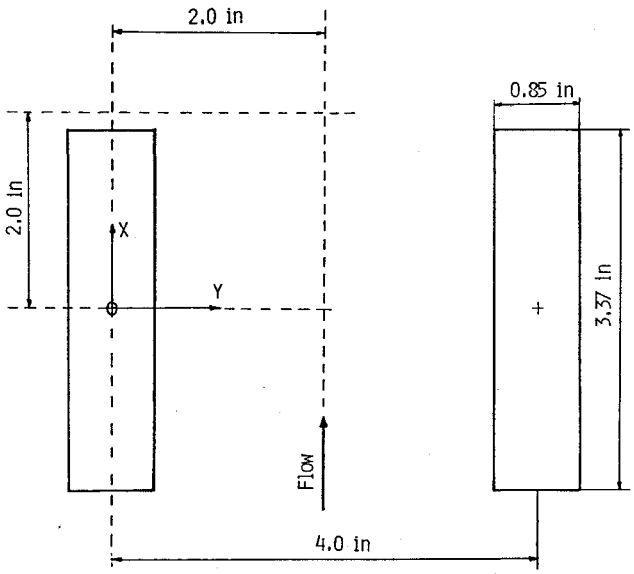

b) Rectangular jets; dimensions and coordinates

Fig. 2 Model details.

Following this channel, there is an 8-cm long contraction, which reduces the cross-sectional area to 2.16×8.57 cm^2 of the jet exit (90-deg jets) and provides a smooth acceleration to the jet exit velocity. When blowers run at maximum power, jet exit velocity was 68.48 m/s (225 ft/s), and the corresponding mass flow rate was 0.134 kg/s for each jet.

Instrumentation

Twelve transducers each connected to a 48-port Scanivalve were used for the pressure distribution experiments. This made it possible to connect 552 pressure ports to the Scanivalves at a time.

A three-dimensional yawhead probe was utilized to obtain mean flowfield measurements in the plumes of the jets. A normal, single hot-wire probe was used for measuring the jet exit turbulence levels when there was no crossflow. These measurements were done without using a linearizer. Turbulence intensities and Reynolds stresses in the plumes of the jets were measured by an X-wire probe. Two constant-temperature anemometers, two linearizers, and a turbulence correlator were used. It is known that for good accuracy with X-wire probes, the probe should be aligned with the mean flow direction at least within 10 deg. Since the probe angle varies considerably for the jet in a crossflow situation, a probe rotator mechanism was necessary. Also, in order to measure all six of the turbulence intensities and Reynolds stresses, and X-wire probe must be rotated around its axis at three different angles—0, 90, and 45 deg. For these reasons, a probe rotator mechanism that also controlled the roll and pitch angles of the probe was designed and built.

A computerized data-acquisition system was used to gather the various experimental data and store them on magnetic disks for subsequent reduction. The computer automatically recorded the tunnel dynamic pressure and temperature, the barometric pressure, the surface pressures induced on the flat plate, and the outputs coming from pitot, yawhead, and hot-wire probes. The computer also controlled the sequential switching of the Scanivalves and the motors of the probe rotator mechanism for the X-wire experiments. The temperature of the jets was measured by a thermocouple and entered into the system manually.

Test Conditions

In order to permit comparison of the results of these experiments with previously obtained results for circular jets (Refs. 6–8, 10, among others), jet-to-freestream velocity ratios of $R = 2.2$, 4, and 8 were chosen for surface pressure distribution experiments. During the experiments, the freestream velocity was changed from 28 to 102 ft/s (8.52 to 31.04 m/s) depending on the jet exit velocity and the jet-to-freestream velocity ratio chosen. The freestream turbulence intensity was about 0.04%. The Reynolds number based on the reference diameter D_{ref} and the freestream velocity was 2.56×10^4 for a 28-ft/s freestream velocity and 9.36×10^4 for 102-ft/s freestream velocity. The Reynolds number at the nozzle, based on flat-plate length up to this point, was 2.5×10^5 for the 28-ft/s freestream velocity and 9.1×10^5 for the 102-ft/s freestream velocity. However, the boundary-layer profile at the jet exit was always turbulent due to early transition caused by the sandpaper strip glued to the flat plate. In Fig. 3, an example can be seen of jet exit velocity profiles that were obtained with the yawhead probe when there is no crossflow. Note that good uniformity and symmetry were obtained. Jet exit turbulence intensity was about 3%.

Experimental Techniques and Data Reduction

Throughout the experiments, different jet-to-freestream velocity ratios were obtained by keeping the jet velocity constant and adjusting the freestream velocity. For the surface pressure distribution tests, tare readings were first obtained by running the tunnel with the jets off and the jet exit areas covered flush to the model surface with an appropriate freestream velocity corresponding to the desired velocity ratio. Pressure readings were then obtained by again running the tunnel with the jets on. The tare readings served to zero out flow disturbances caused by any small irregularities on the surface of the model. Nondimensional pressure coefficients

$$C_p = \frac{p - p_\infty}{q_\infty} \tag{1}$$

were obtained for jet-off and jet-on cases for each R, and the data is presented as

$$\Delta C_p = (C_{p_{\text{jet on}}} - C_{p_{\text{jet off}}}) \tag{2}$$

Results were plotted as isobars with a computer program, which is explained in Ref. 26.

Mean velocity vector plots were obtained by using the yawhead probe. These tests were done for side-by-side dual jets only. Only one of the jets was surveyed, and it was assumed that the flow was symmetrical. In order to minimize

flow angularity with respect to the yawhead probe at different measurement locations, the yawhead probe was kept at a 45-deg pitch angle with respect to the model surface. A computer program taken from Ref. 25 was used for data reduction. This program is based on calibration of the probe and is valid up to 60-deg flow angularities with respect to the probe.

Turbulence measurements in the jet plume were made with the X-wire probe. At each measurement location, the flow direction was known from the previously made yawhead measurements. Before a measurement, the X-wire probe was aligned with the flow direction by changing the pitch angle of the probe. Then data was read at 0-, 90-, and 45-deg roll angles of the probe. The turbulence quantities were first obtained in the probe coordinates; they are then transferred into the usual Cartesian coordinate system for plotting. The normalization was with the local total mean velocity.

Results

Pressure Distributions

The results of the surface pressure distribution tests will be presented as ΔC_p isobars. In the figures, thin isobar lines are drawn at $\Delta C_p = 0.2$ intervals, and thick isobar lines are drawn at $\Delta C_p 1.0$ intervals. An exception to this rule is Fig. 7, where

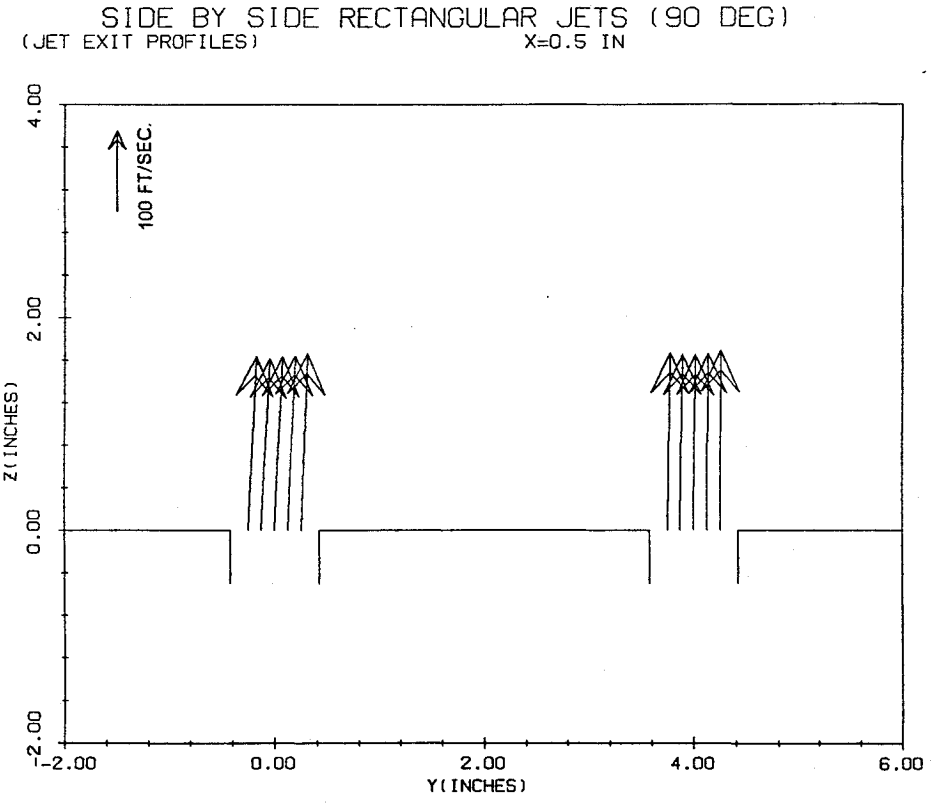

Fig. 3 Jet exit velocity profiles.

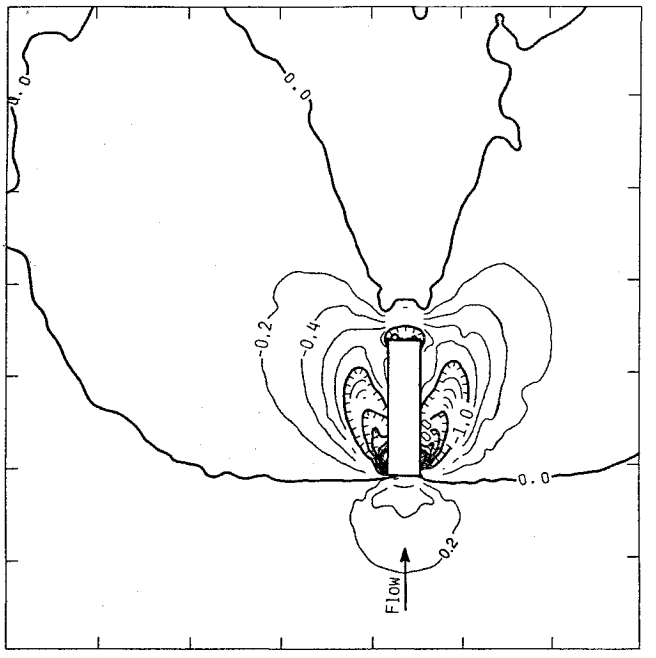

Fig. 4a Surface pressures, 90 deg rectangular jet, R = 2.2; single jet.

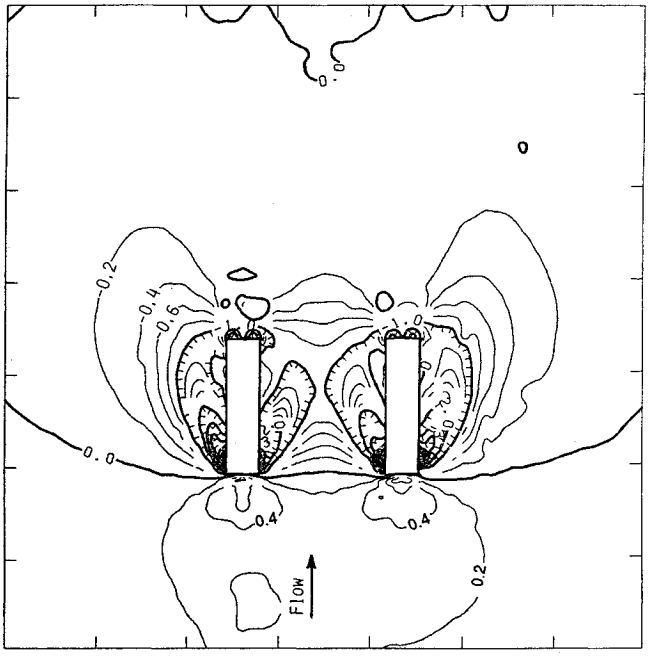

Fig. 4b Surface pressures, 90 deg rectangular jet, R = 2.2; side-by-side.

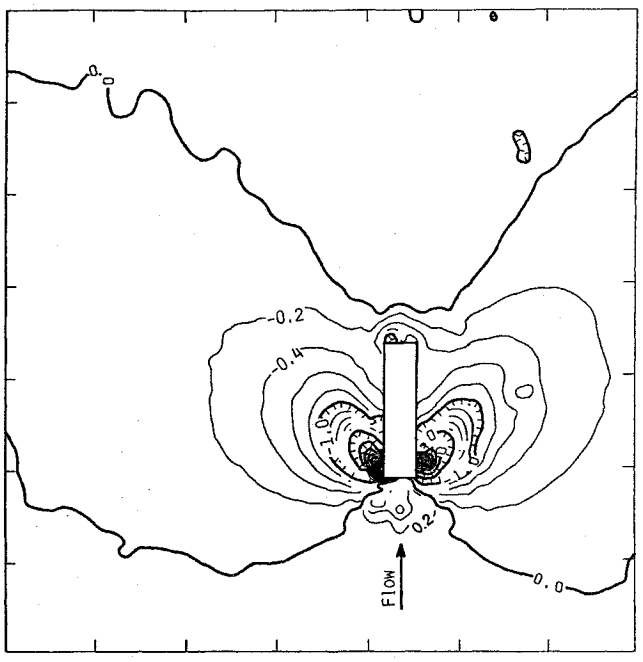

Fig. 5a Surface pressures, 90 deg rectangular jet, $R = 4.0$; single jet.

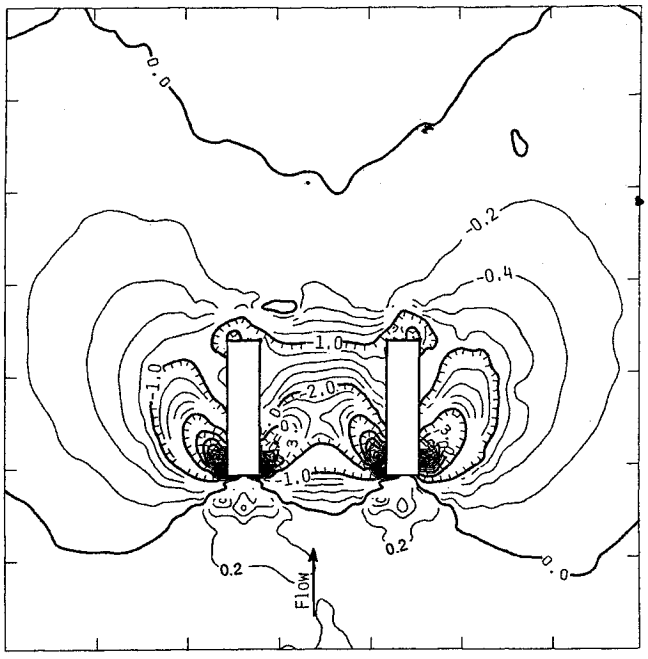

Fig. 5b Surface pressures, 90 deg rectangular jet, $R = 4.0$; side-by-side.

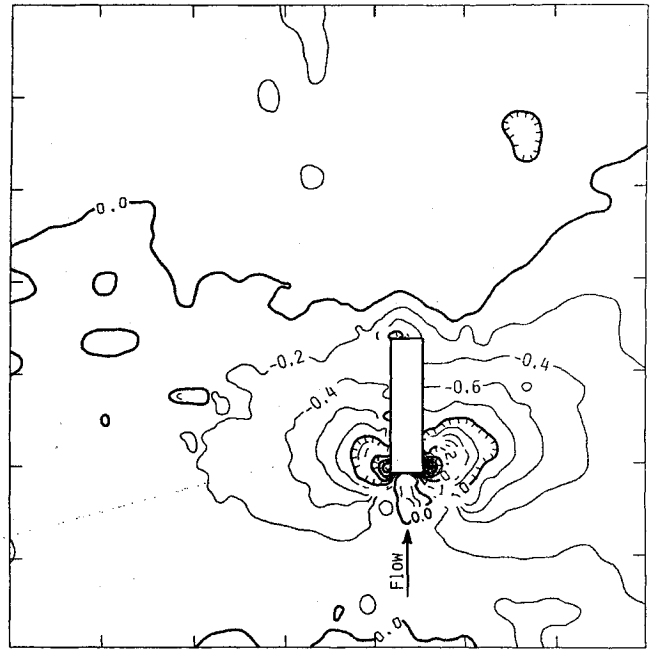

Fig. 6a Surface pressures, 90 deg rectangular jet, $R = 8.0$; single jet.

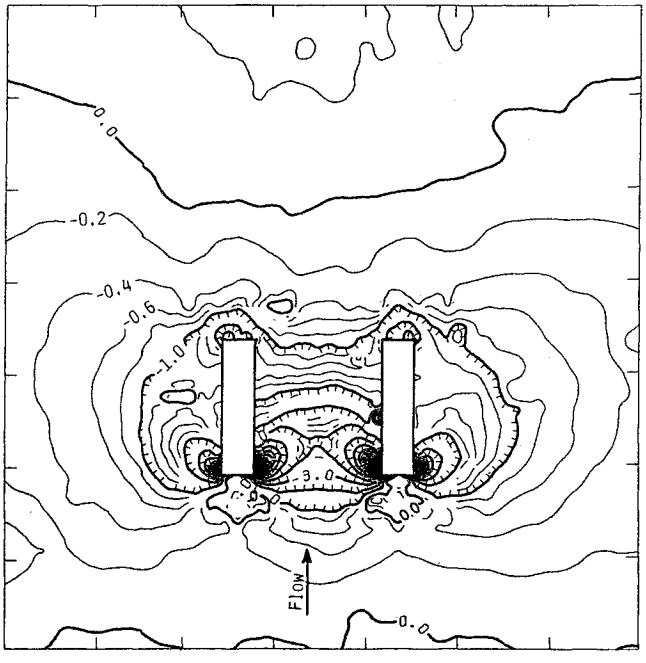

Fig. 6b Surface pressures, 90 deg rectangular jet, $R = 8.0$; side-by-side.

thin lines are drawn at $\Delta C_p = 0.4$ intervals, and thick lines are drawn at $\Delta C_p = 2.0$ intervals. All of the results are plotted with the same scale (except Fig. 7), so the dimensions and areas are comparable.

90-Deg Rectangular Jets

Results for 90-deg rectangular jets can be seen in Figs. 4–7. In the upper part of Fig. 4, one can see the results for a single jet with $R = 2.2$. There is a large area influenced with negative pressures that extends toward the sides and downstream from the jet leading edge. In front of the jet, there is a positive pressure region due to deceleration of the freestream. There are very high negative pressures at both sides of the front corner, which are due to sharp and sudden changes in the magnitude and direction of the velocity vector and local flow separation. Although lower in magnitude, there is another negative pressure region around the rear corners. This should also be due to flow separation and other effects. The pressure distribution is quite symmetric, and the high negative pressures in the close vicinity of the jet decay rather fast. By increasing jet-to-freestream velocity ratio to 4.0, the downstream extent of the negative pressures reduces, but their upstream extent increases. This can be seen by observing the shift of the pressure line labeled "0.0" from Fig. 4a to Fig. 5a. The negative peak pressures at the front corners are also larger. The effect of the rear corners reduces. The decay of negative pressures is slower and this is why the $\Delta C_p = -0.2$ line covers a larger area. There is again a positive region in front of the jet; however, this region has a smaller area compared to $R = 2.2$. Increasing the velocity ratio to 8 as shown in Fig. 6a further reduces the

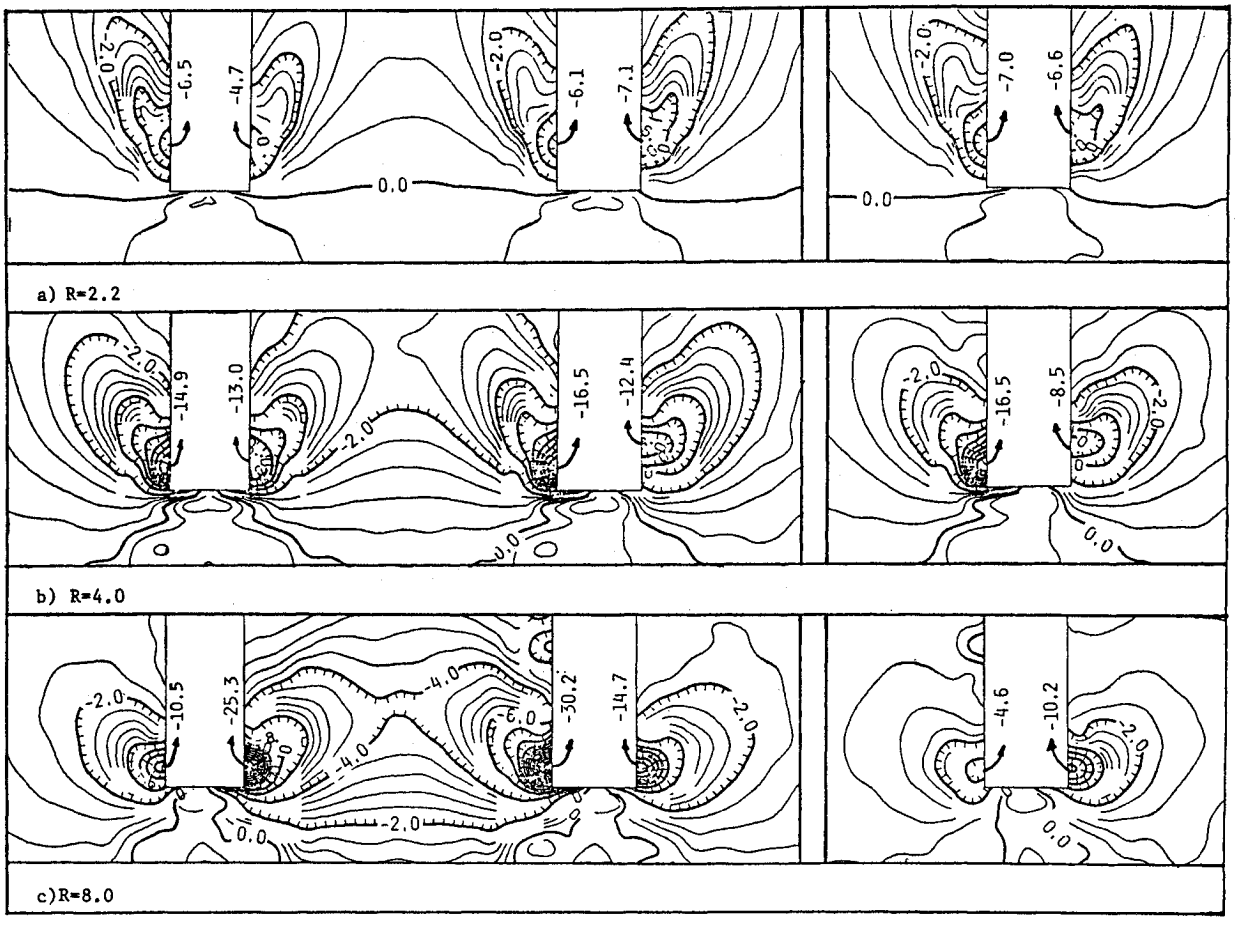

Fig. 7 Surface pressure, 90 deg rectangular jets, enlarged front area.

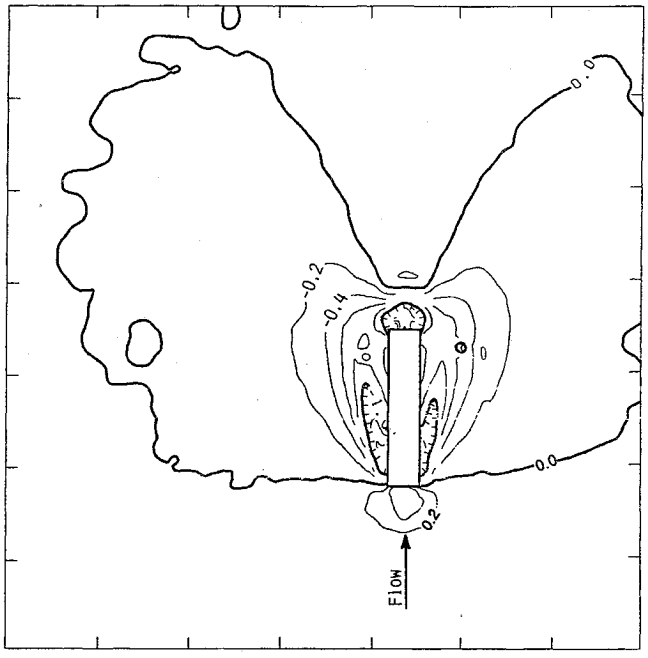

Fig. 8a Surface pressures, 60 deg rectangular jet, $R = 2.2$; single jet.

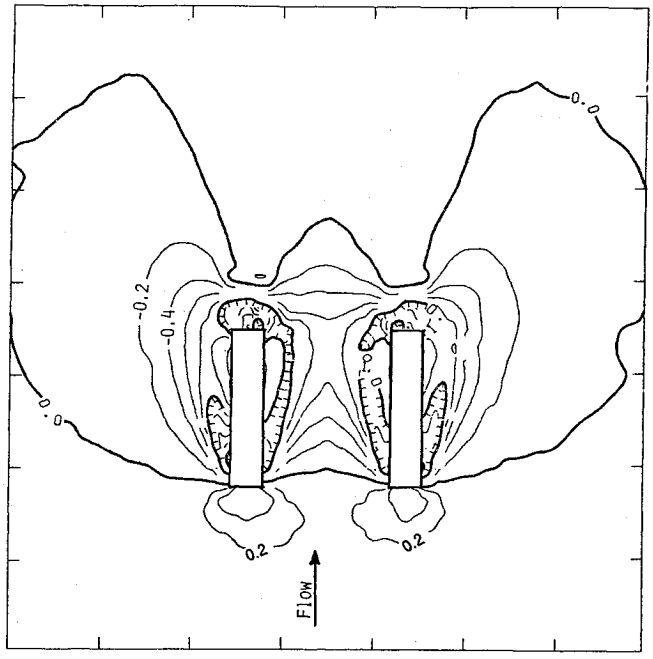

Fig. 8b Surface pressures, 60 deg rectangular jet, $R = 2.2$; side-by-side.

downstream extent of the negative pressures and increases their extent toward the sides and upstream. Again, there is a positive pressure region in front of the jet, which is surrounded by the negative pressure region from all sides. Decay of the negative pressures is even slower. The sharp peaks at the front corners seem to be of less magnitude compared to the $R = 4$ case.

For 90-deg rectangular jets, the flow structure in the close vicinity of the front corners is quite complicated, so these areas are enlarged in Fig. 7. At the right-hand side of Fig. 7,

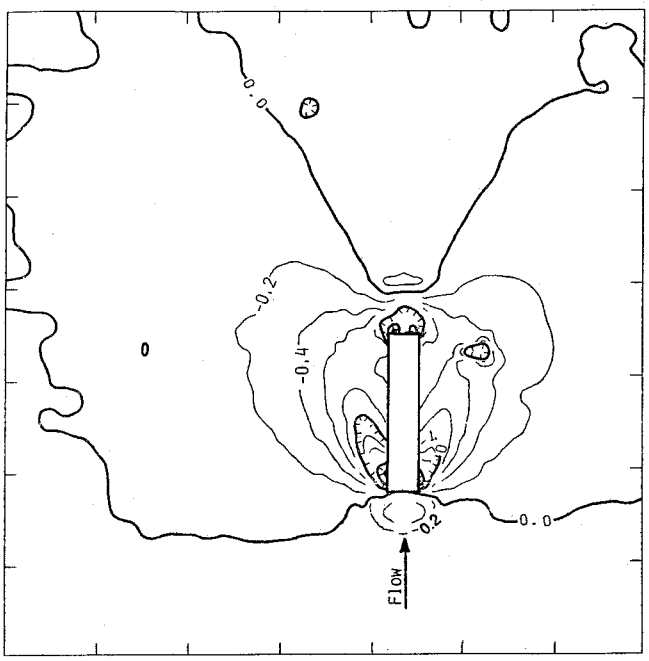

Fig. 9a Surface pressures, 60 deg rectangular jet, $R = 4.0$; single jet.

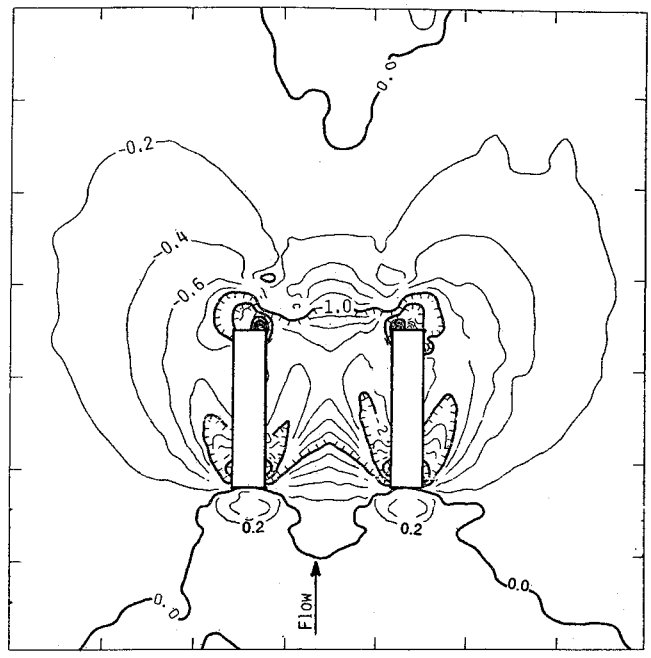

Fig. 9b Surface pressures, 60 deg rectangular jet, $R = 4.0$; side-by-side.

compare the front corner regions of the single jets for $R = 2.2$, 4, and 8. The asymmetry seen for $R = 4$ and 8 can be due either to imperfections of the jet exit profile or to uncertainty caused by an insufficient number of pressure taps. The locations of the negative peaks are a little closer to the front edge for $R = 4$ and 8 when compared to $R = 2.2$. The magnitude of the peaks increases when the velocity ratio increases from 2.2 to 4. They decrease again when the velocity ratio is further increased to $R = 8$. One argument is quite helpful to understand what is happening by changing the velocity ratio. The $R = 2.2$ case is closer to the case of $R = 0$. For $R = 0$, there would not be positive or negative pressure regions on the flat-plate surface. The case $R = 8$ is closer to $R = \infty$, and for $R = \infty$ there would be negative pressure areas around the jet exit that are distributed symmetrically. However, there would not be sharp negative corner peaks caused by the interaction of two streams. The case $R = 2.2$ has the highest freestream dominancy when compared to $R = 4$ and 8. That is why, for this case, one does not observe upstream extension of negative pressure areas. Increasing the velocity ratio reduces the dominancy of the freestream and increases the dominancy of the jet on the pressure distribution.

Results for 90-deg side-by-side, dual rectangular jets are presented in Figs. 4b, 5b, and 6b for $R = 2.2$, 4, and 8. Again, enlarged front corner regions can be seen in Fig. 7. Most of the arguments made for the single jets are also valid for this configuration. Dual jets produce a larger negative pressure area, particularly toward the downstream. Again, the decay of negative pressure slows down by increasing velocity ratio. This is clear when one observes, for example, how the area covered by the $\Delta C_p = -0.2$ line enlarges with increasing velocity ratio. Also, the upstream extent of negative pressures increases with increasing velocity ratio.

The flow between two jets and the influence of each jet on the other causes additional complications of the flow structure for dual jets. These effects increase with increasing velocity ratio. Looking at Fig. 4b for $R = 2.2$, one can still say that there is some symmetry on the inner and outer sides of each jet. This is no longer true for $R = 4$ and 8. For these cases, symmetry is valid with respect to a line passing from the middle of the two jets and parallel to the freestream. However, the inner and outer sides of each jet are not symmetric. For example, if one compares the inner corner peaks to the outer corner peaks for $R = 8$ in Fig. 7, the inner peaks have magnitudes like -25.3 and -30.2 and the outer peaks -10.5 and -14.7. The outer side of each jet behaves more like one side of a single jet, which is not true for the inner sides. Also, negative pressures with higher magnitude and larger area occur over the surface. Comparing the areas covered by the $\Delta C_p = -1.0$ line for a single jet ($R = 4$), one can see that for dual jets, the line covers an area larger than twice the area covered for a single jet. By further increasing the velocity ratio (even more than 8), the effects of channel flow between the jets would start reducing, but the effects of one jet on the other will continue to increase due to weaker crossflow and stronger jets.

60-Deg Rectangular Jets

Pressure distribution results for 60-deg injection are presented in Figs. 8–10. These results are qualitatively similar to the 90-deg rectangular jet results. The same things can be said about the effects of velocity ratio or the differences between single and dual jets. However, the interaction of 60-deg jet(s) with the freestream is smoother, thus producing lower magnitude negative pressure areas in the near vicinity of jet exits. Comparing single jet results for $R = 4$ for 90 and 60 deg (Figs. 5a and 9a), one can see that the areas covered by $\Delta C_p = 0.0$ line have not been influenced much. However, the area covered by $\Delta C_p = -0.2$ line is lesser, and the area covered by $\Delta C_p = -1.0$ line is even less for 60-deg jets.

For the 60-deg jets, one no longer sees dramatically high negative pressure peaks around the front corners. Instead of negative pressure peaks to -16.0 as for 90-deg jets, the maximum for 60-deg jets is about -4.0. The importance of the rear corners seems to increase for the 60-deg jets. One observes higher magnitude negative pressures around these corners. Compare dual rectangular jets for $R = 4$ from Figs. 5b and 9b. Again, the area covered with lower magnitude negative pressures does not seem to be influenced too greatly. However, the area covered by the $\Delta C_p = -1.0$ line is clearly less for 60-deg jets, and the area covered by $\Delta C_p = -2.0$ line is much less. The inside, rear corners of the 60-deg dual jets produce negative pressures of roughly -5.0 in magnitude, which is not found for 90-deg jets at $R = 4.0$. It seems that there is a strong flow interaction around the rear corners for 60-deg jets. These same things can be said for the other velocity ratios, too. However, for $R = 2.2$ even the low magnitude ΔC_p lines, such as 0.0 and -0.2, cover a smaller area (compare Fig. 4a to Fig. 8a, and Fig. 4b to Fig. 8b). This might be due to stronger

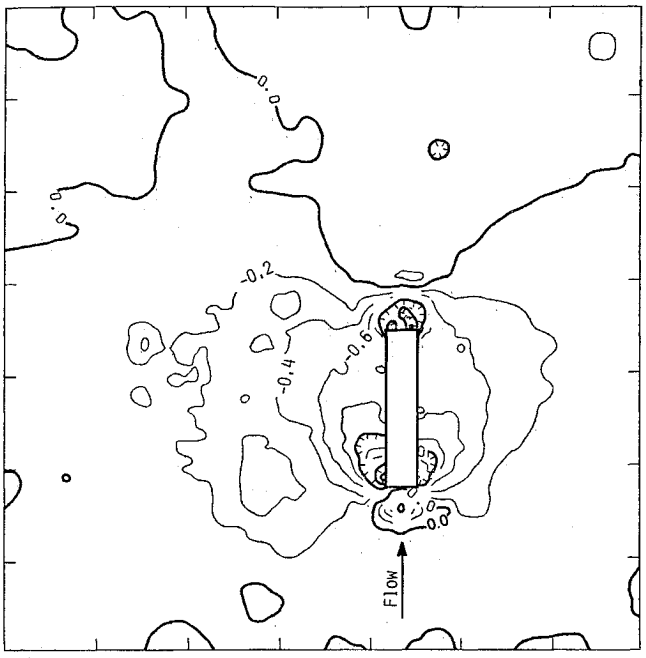

Fig. 10a Surface pressures, 60 deg rectangular jet, $R = 8.0$; single jet.

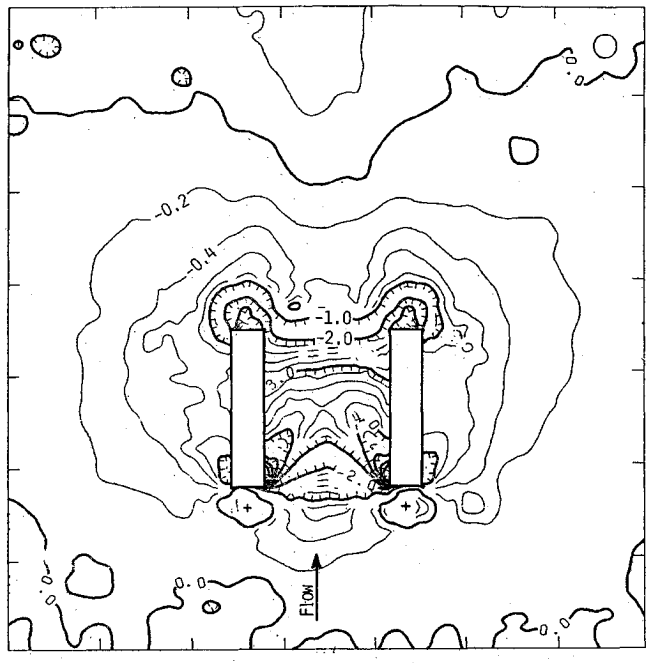

Fig. 10b Surface pressures, 60 deg rectangular jet, $R = 8.0$; side-by-side.

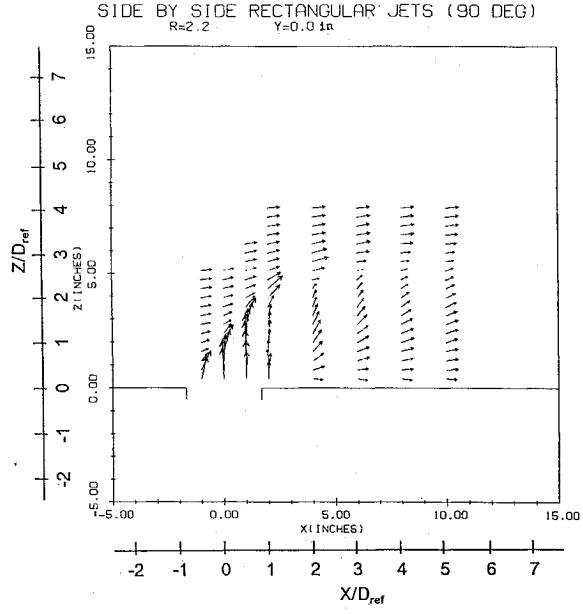

Fig. 11 Mean flowfield, 90 deg side-by-side dual rectangular jet, $R = 2.2$; $Y/D_{ref} = 0.0$.

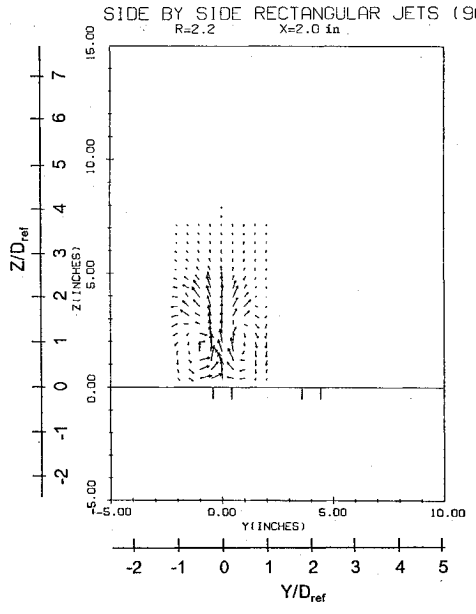

Fig. 12 Mean flowfield, 90 deg side-by-side dual rectangular jet, $R = 2.2$; $X/D_{ref} = 1.026$.

crossflow effects. As with the 90-deg jets, the 60-deg jets produced symmetric pressure distributions.

Mean Flowfield Measurements

Mean flowfield measurement results are presented in Figs. 11–16. These measurements were done for 90- and 60-deg side-by-side dual rectangular jets. For 90-deg jets, the data were obtained for $R = 2.2$ and 4.0 and for 60-deg jets for $R = 4.0$. From Fig. 11 for $R = 2.2$ and for 90-deg jets, one can see that the penetration height of the center of the jet plume is about 15 cm (6 in.) ($Z/D_{ref} = 3$). Little actual flow reversal is seen at this measurement station. From the $X = 5$ cm (2 in.) ($X/D_{ref} = 1$) cross section in Fig. 12, vortical flow formation at both sides of the jet is quite clear. At low Z locations, the jet sucks in the outside air, and for high Z locations, the jet spreads out. The same type of flow can be observed for $R = 4$ from Figs. 13 and 14. For that case, the penetration height is about 30 cm (12 in.) ($X/D_{ref} = 6.5$), and somewhat more flow reversal is evident right behind the jet column.

In Figs. 15 and 16, the results for 60-deg jets at $R = 4$ can be seen. Of course, interaction of the two streams is smoother, and the jet penetrates to a lower Z distance compared to 90-deg injection. From Fig. 15, one can say that the penetration height is about 23 cm (9 in.) ($Z/D_{ref} = 4.5$). There is no flow reversal. The vortices in the plume are much smaller than for the 90-deg case.

Turbulence Measurements

Results of turbulence measurements are presented in Figs. 17–20. The measurements were done for 90- and 60-deg dual jets and $R = 4$. For both cases, data were taken for only one plane, i.e., $Y/D_{ref} = 0.0$. Local total mean velocity was used

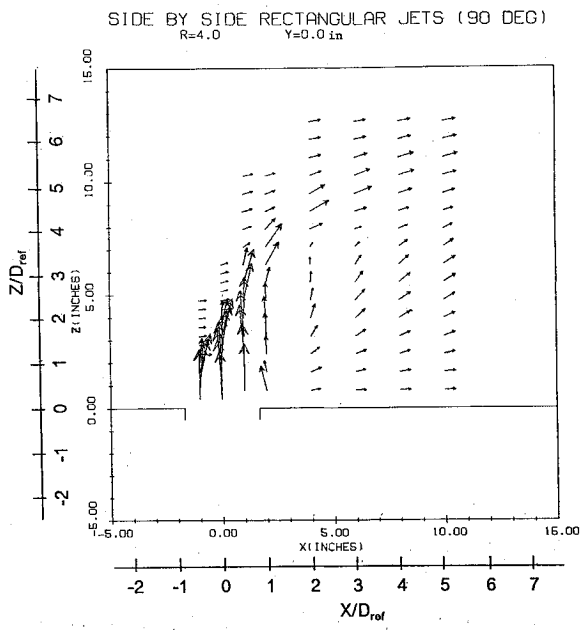

Fig. 13 Mean flowfield, 90 deg side-by-side dual rectangular jet, $R = 4.0$; $X/D_{ref} = 0.0$.

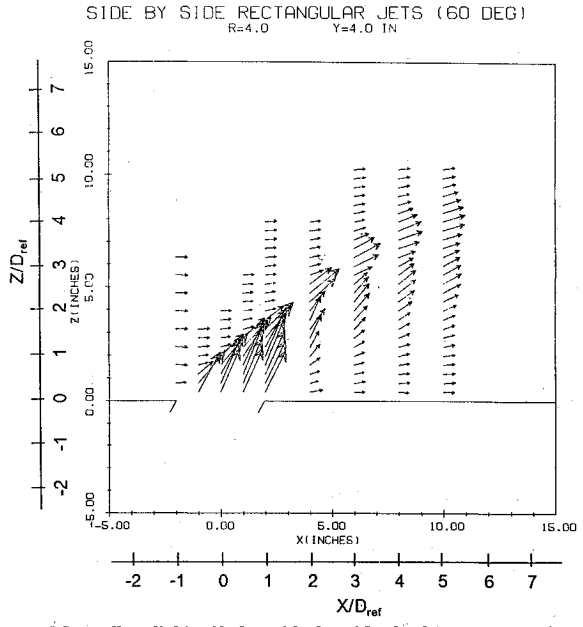

Fig. 15 Mean flowfield, 60 deg side-by-side dual rectangular jet, $R = 4.0$; $X/D_{ref} = 2.051$.

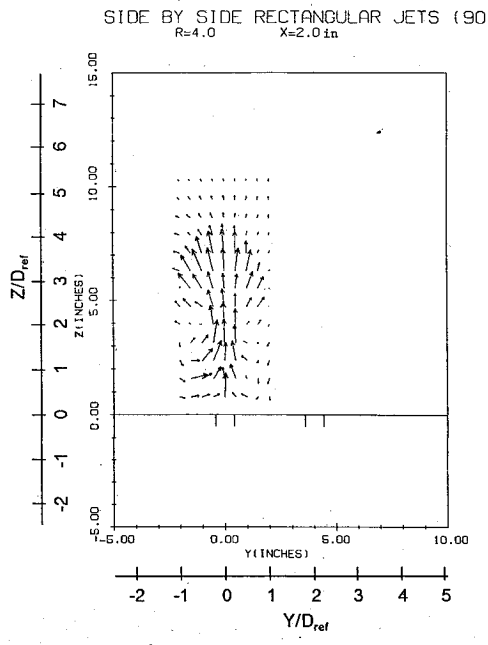

Fig. 14 Mean flowfield, 90 deg side-by-side dual rectangular jet, $R = 4.0$; $X/D_{ref} = 1.026$.

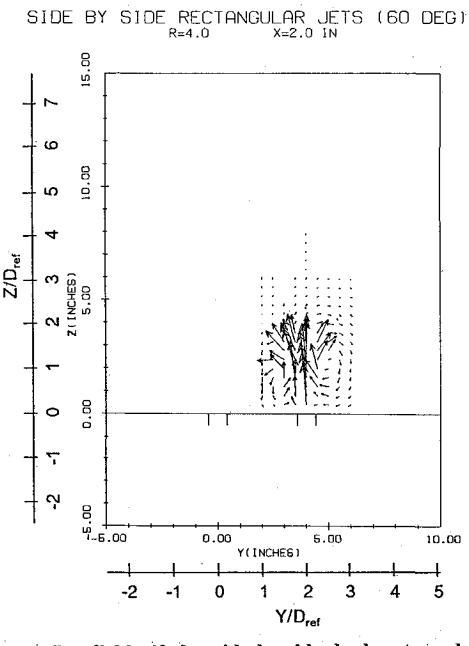

Fig. 16 Mean flowfield, 60 deg side-by-side dual rectangular jet, $R = 4.0$; $X/D_{ref} = 1.026$.

for normalization of the turbulence data. If one looks at these turbulence data together with the previously presented mean flow data, the understanding of the results can be easier.

90-Deg Side-by-Side Dual Rectangular Jets

In Fig. 17, we show turbulence intensities in the X, Y, and Z directions ($\tilde{u}$, $\tilde{v}$, $\tilde{w}$). One can see that $\tilde{u}$ and $\tilde{w}$ have a similar behavior, whereas $\tilde{v}$ behaves differently. It seems that in jet-dominated regions, $\tilde{u}$ and $\tilde{w}$ are higher, and in wake-dominated regions, $\tilde{v}$ is higher. Both the jet and the freestream are actually low turbulence flows. Therefore, the jet core and freestream-dominated regions have low turbulence intensities. Turbulence increases with increased mixing and interaction of each stream. For $X/D_{ref} = 0.0$, all three turbulence intensities increase with increasing Z, and they have peak values around $Z/D_{ref} = 3$. Then, they start decreasing to their freestream values. Peak values are around 40% for $\tilde{u}$, 30% for $\tilde{w}$, and 15% for $\tilde{v}$. The $\tilde{v}$ has considerably lower values than the other two. For low Z locations, turbulence intensities are below 5%. These areas actually correspond to the core of the jet. The same type of argument is true for $X/D_{ref} = 0.53$. More data points fell into the core of the jet. Peak turbulence intensities shift to around the $Z/D_{ref} = 4$ location. Peak values are about 45% for $\tilde{u}$, 40% for $\tilde{w}$, and 15% for $\tilde{v}$. These peak values occur at the outer edge of the jet at the mixing layer between the jet and freestream. At $X/D_{ref} = 1.05$, one cannot observe the effect of a jet core anymore. Instead, low Z locations are now under the influence of the wake flow behind the jet and also under the influence of the vortex flows separating from both sides of the jet. In this wake-dominated region, all three turbulence intensities have values around 20–30%. By coming closer to the jet-dominated region, $\tilde{u}$ and $\tilde{w}$ start increasing and $\tilde{v}$ starts decreasing. All of the turbulence intensities again have their peak values in the outer mixing region of the jet and freestream. The peak for $\tilde{v}$ is less pronounced. Peak values for $\tilde{u}$ and $\tilde{w}$ are about 45% and for $\tilde{v}$ about 20%, which is lower

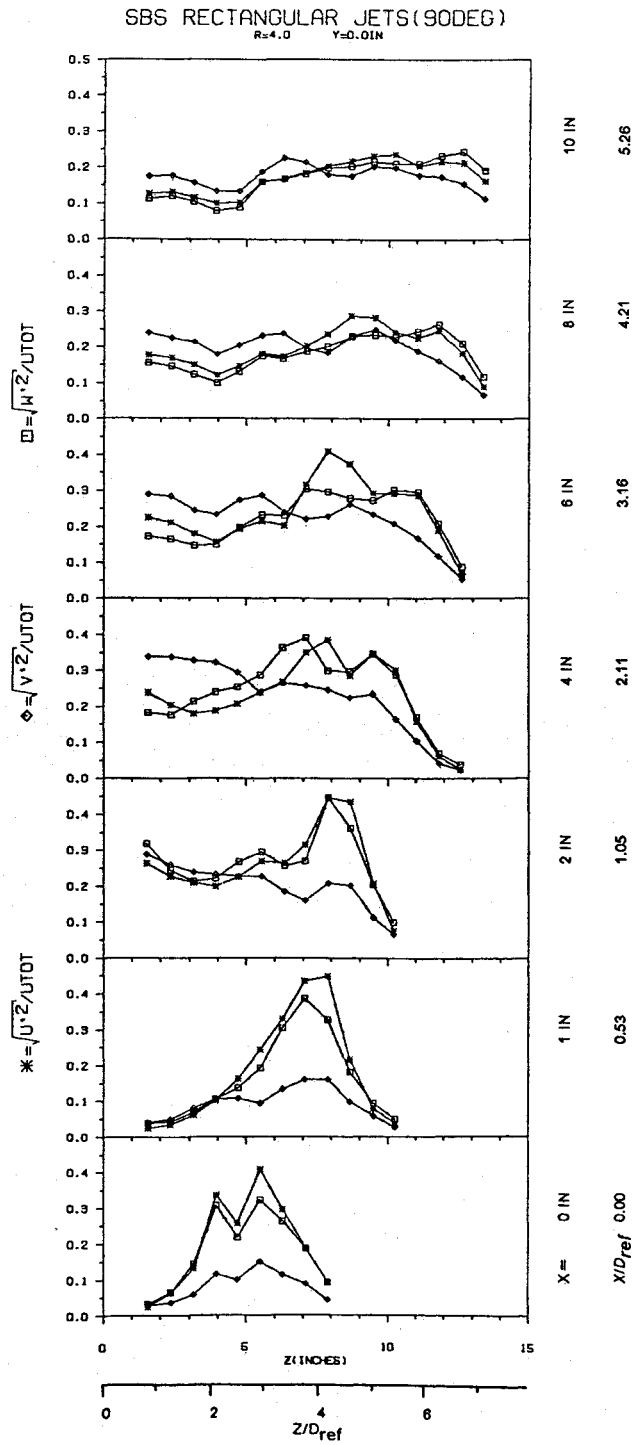

Fig. 17 Turbulence intensities, 90 deg side-by-side dual rectangular jet, $R = 4.0$.

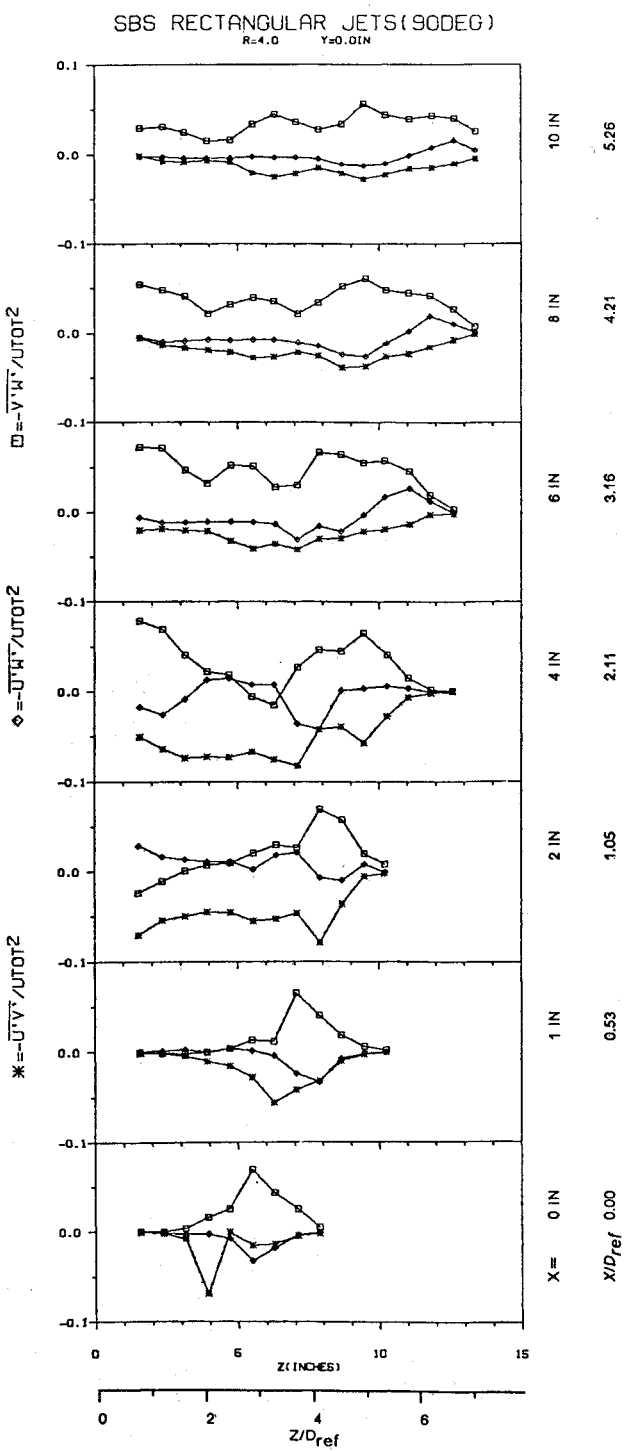

Fig. 18 Turbulent stresses, 90 deg side-by-side dual rectangular jet, $R = 4.0$.

than the value of $\tilde{v}$ in the wake region. For $X/D_{ref} = 2.11$, $\tilde{v}$ is considerably larger than $\tilde{u}$ and $\tilde{w}$ in the wake region, and it decreases smoothly when coming to the jet region. For $\tilde{u}$ and $\tilde{w}$, two peaks are pronounced—one at the lower edge of the jet and the other at the outer edge of the jet. The peaks at the lower edge are about 40%, and the ones at the outer edge are about 35%. By going downstream, the differences between the jet and wake regions diminish. These two actually start becoming the same region. Turbulence intensities decay further, and they start becoming more isotropic.

In Fig. 18, Reynolds stresses are presented. The $-\widetilde{uw}$ is usually smaller in magnitude compared to $-\widetilde{uv}$ and $-\widetilde{vw}$. It is seen that $-\widetilde{uv}$ usually takes negative values, and $-\widetilde{uw}$ usually takes positive values. For $X/D_{ref} = 0.0$, 0.53, and 1.05, $-\widetilde{uv}$ makes a negative peak, and $-\widetilde{vw}$ makes a positive peak. For $X/D_{ref} = 2.11$, the situation is a little more complicated because of the increased effect of the wake. By going further downstream, the curves get smoother.

60-Deg Side-by-Side Dual Rectangular Jets

In Fig. 19, turbulence intensities are presented for the 60-deg jets. The functional behavior of the curves are quite similar to that for the 90-deg jets. The profiles are a little compressed in the Z direction, because the 60-deg jets have lower penetration height. The jet has higher velocities than the freestream even for the downsteam locations such as $X/D_{ref} = 4.21$ and 5.26. For that reason, the shear layer between the jet and the freestream produces observable peak

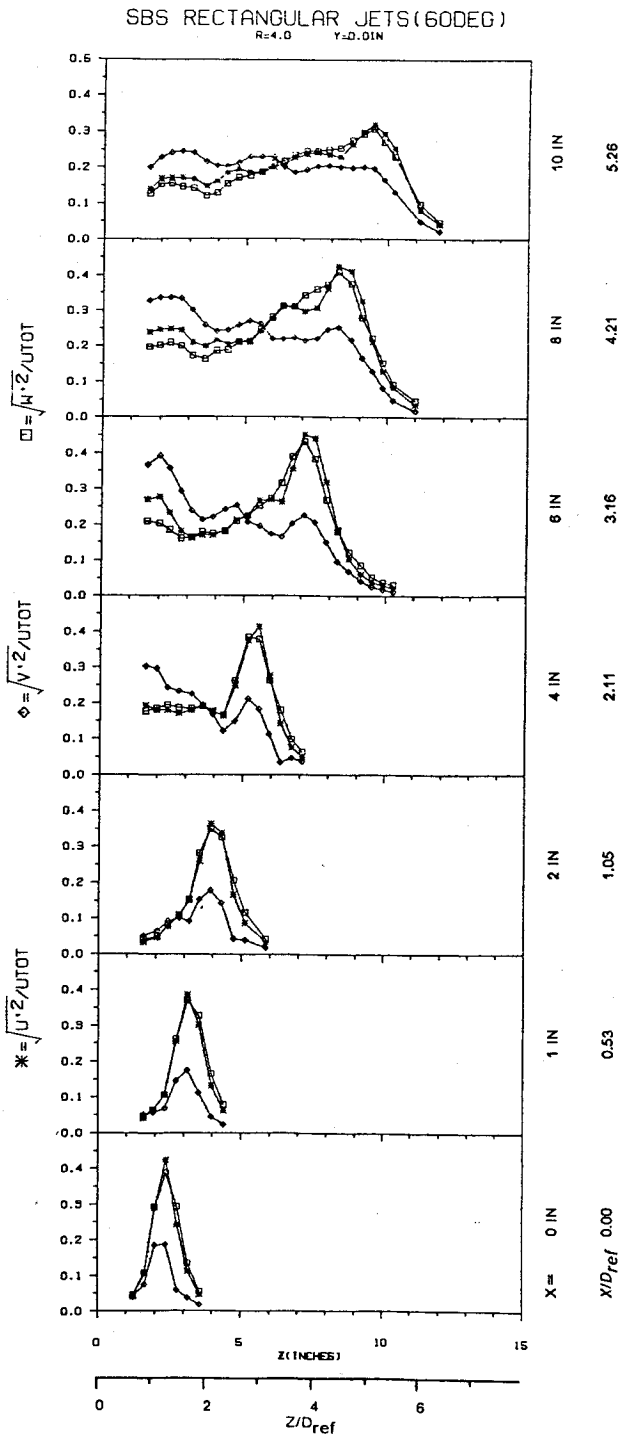

Fig. 19 Turbulence intensities, 60 deg side-by-side dual rectangular jet, $R = 4.0$.

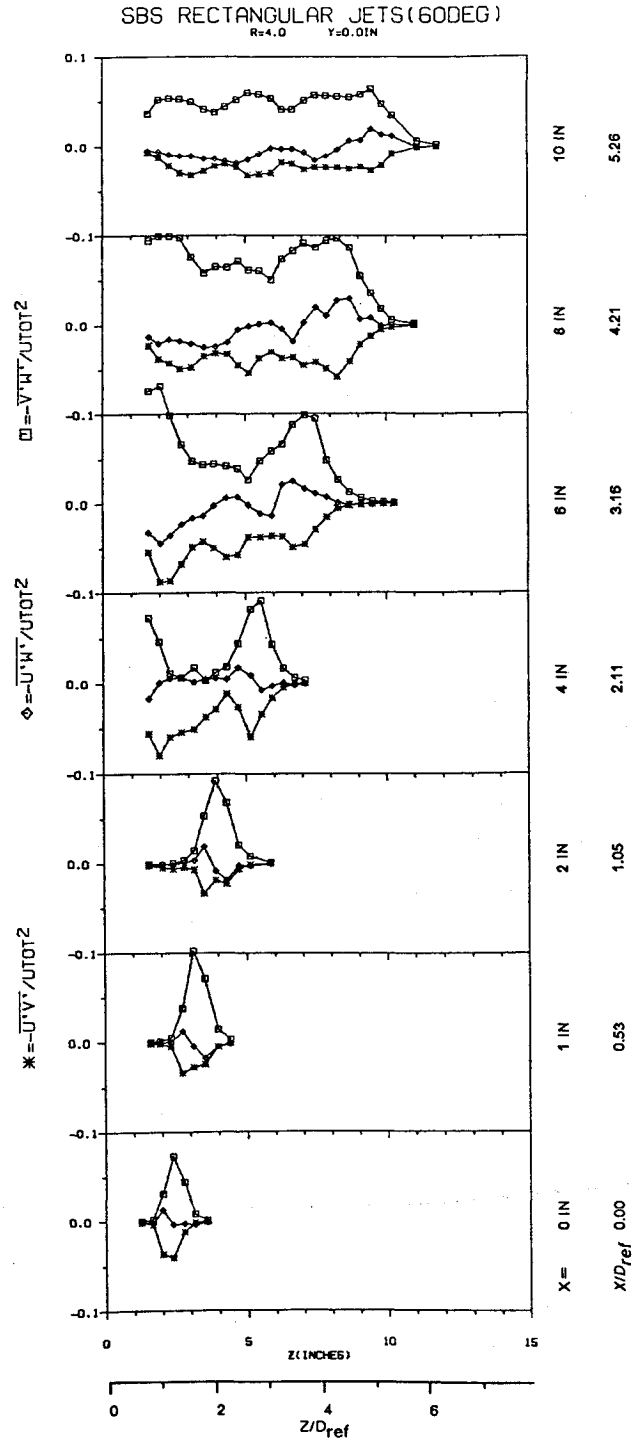

Fig. 20 Turbulence stresses, 60 deg side-by-side dual rectangular jet, $R = 4.0$.

values for $\tilde{u}$ and $\tilde{w}$ at these stations. Again, $\tilde{v}$ takes higher values in the wake-dominated region and lower values in the jet-dominated region. This can be judged as logical, because for the wake-dominated region the measurement plane is presumed to be the symmetry plane for two counter-rotating vortices. Two flows with opposite direction Y mean component velocities meet each other in this plane, therefore velocity fluctuations in the Y direction are high. For the jet-dominated region, two flows with almost no Y mean component velocities hit each other (jet and freestream). The directions and magnitudes for these two flows in the X–Z plane are different. This causes higher fluctuating velocities in the X and Z directions.

In Fig. 20, results for the Reynolds stresses can be seen. The functional behavior of $-\widetilde{uv}$ and $-\widetilde{vw}$ are again quite similar to that for 90-deg jets. For $X/D_{ref} = 0.53$ and 1.05, $-\widetilde{uw}$ makes one positive and one negative peak. This is not very clear for 90-deg jets.

Table 2 Comparison of surface pressures for single jets for $R = 4.0$. Circular jet data is taken from Ref. 23

Jet type	A_{-1}/A_{exit}	$A_{-0.2}/A_{exit}$
90-deg rectangular	1.90	14.33
60-deg rectangular	0.68	10.86
90-deg circular	4.31	22.66

Discussion

In Table 2, single-jet pressure distribution results are compared for $R = 4$. In this table, results for a 90-deg single circu-

lar jet from Ref. 23 are also included. The ratios of the areas covered by the $\Delta C_p = -1$ line and the $\Delta C_p = -0.2$ line to jet exit area are presented. For the 60-deg rectangular jet, instead of the jet exit area, the projection of this area on a plane perpendicular to jet axis is taken. Negative pressure areas were smallest for the 60-deg jet and largest for the circular jet of Ref. 23. The circular jet of Ref. 23 had uniform velocity profile and low exit turbulence like the present rectangular jets. Comparisons can also be made with other previous circular jet results, such as, the present dual jet results can be compared with the dual circular jet results of Ref. 2. The main difference of rectangular jets from the circular ones is the sharp negative peak values of ΔC_p around the front corners. The maximum negative pressures are lower for circular jets, and are located at the left and right sides of the jet. For the side-by-side dual configuration, the streamwise rectangular jets can be brought closer to each other with less blockage to the freestream than the circular ones. The negative pressure area behind the circular jets extends further downstream. However, the decay is smoother. Streamwise-aligned rectangular lift jets can provide the same thrust with less surface interaction. The sharp negative pressure peaks around the front corners of the rectangular jets can likely be reduced by rounding the corners.

Acknowledgment

This work was supported by NASA Ames Research Center. Mr. K. Aoyagi was the technical monitor.

References

[1]Schetz, J. A., "Injection and Mixing in Turbulent Flow", *Progress in Astronautics and Aeronautics*, Vol. 68, AIAA, New York, 1980, Chap. 6.

[2]Abramovich, G. N., *The Theory of Turbulent Jets,* MIT Press, Cambridge, MA, 1960 (English Edition).

[3]Lee, C. C., "A Review of Research on the Interaction of a Jet with an External Crosstream," TN R-184, Contract DA-01-021-AMC-11528 (z), Research Lab., Brown Engineering Co., Inc., March 1966.

[4]Garner, J. E., "A Review of Jet Efflux Studies Application to V/STOL Aircraft," Arnold Engineering Development Center, AEDC-TR-67-163, U.S. Air Force, Sept. 1967.

[5]Perkins, S. C., Jr. and Mendenhall, M. R., "A Study of Real Jet Effects on the Surface Pressure Distribution Induced by a Jet in a Crossflow," NASA CR-166150 (N81-23029), March 1981.

[6]Schetz, J. A., Jakubowski, A. K., and Aoyagi, K., "Jet Trajectories and Surface Pressures Induced on a Body of Revolution with Various Dual Jet Configurations," *Journal of Aircraft*, Vol. 20, Nov. 1983, pp. 975-982.

[7]Schetz, J. A., Jakubowski, A. K., and Aoyagi, K., "Surface Pressures Induced on a Flat Plate with In-Line and Side-by-Side Dual Jet Configurations," *Journal of Aircraft*, Vol. 21, July 1984, pp. 484-490.

[8]Moore, C. L. and Schetz, J. A., "Effects of Nonuniform Velocity Profiles on Dual Jets in a Crossflow," AIAA Paper 85-1674, July 1985.

[9]Kavsaoglu, M., Schetz, J. A., and Jakubowski, A. K., "Dual Rectangular Jets from a Flat Plate in a Crossflow," AIAA Paper 86-0477, Jan. 1986.

[10]Jakubowski, A. K., Schetz, J. A., Moore, C. L., and Joag, R., "Effects of Velocity Profile and Inclination on Dual-Jet-Induced Pressures on a Flat Plate in a Crosswind," NASA CR-177361, Oct. 1985.

[11]Crabb, D., Durao, D. F. G., and Whitelaw, J. H., "A Round Jet Normal to a Crossflow," *Transactions of the ASME, Journal of Fluids Engineering*, Vol. 103, March 1981, pp. 142-152.

[12]Isaac, K. M. and Jakubowski, A. K., "Experimental Study of the Interaction of Multiple Jets with a Crossflow," *AIAA Journal*, Vol. 23, Nov. 1984, pp. 1679-1683.

[13]Bradbury, L. J. S. and Wood, M. N., "The Static Pressure Distribution Around a Circular Jet Exhausting Normally from a Plane Wall into an Airstream," Aeronautical Research Council CP822, 1965.

[14]Fearn, R., Kalota, C., and Dietz, W. E., Jr., "A Jet/Aerodynamic Surface Interference Model," *Proceedings of V/STOL Aircraft Aerodynamics Workshop at NADC*, Monterey, CA, May 1979.

[15]Volger, R. D., "Surface Pressure Distributions Induced on a Flat Plate by a Cold-Air Jet Issuing Perpendicularly from the Plate and Normal to a Low-Speed Freestream Flow," NASA TN D-1629, March 1963.

[16]Fearn, R. L. and Weston, R. P., "Induced Pressure Distribution of a Jet in a Crossflow," NASA TN D-7916, June 1975.

[17]Mosher, D. K., "An Experimental Investigation of a Turbulent Jet in a Crossflow," Ph. D. Thesis, Georgia Inst. of Technology, GA Dec. 1970; Rept. GIT-AER-70-715.

[18]Weston, R. P. and Thames, F. C., "Properties of Aspect Ratio 4.0 Rectangular Jets in a Subsonic Crossflow," *Journal of Aircraft,* Vol. 16, Oct. 1979, pp. 701-707.

[19]Snyder, P. and Orloff, K. L., "Three-Dimensional Laser Doppler Anemometer Measurements of a Jet in a Crossflow," NASA TM-85997, Sept. 1984.

[20]Andreopoulos, J. and Rodi, W., "Experimental Investigation of Jets in a Crossflow," *Journal of Fluid Mechanics,* Vol. 138, 1984, pp. 93-127.

[21]Andreopoulos, J., "On the Structure of Jets in a Crossflow," *Journal of Fluid Mechanics,* Vol. 157, 1985, pp. 163-197.

[22]Kavsaoglu, M. S., "Jets in a Crossflow Including the Effects of Dual Arrangements, Angle, Shape, Swirl, and High Turbulence," Ph. D. Dissertation, Virginia Polytechnic Inst. and State Univ., VA, 1987.

[23]Kavsaoglu, M. S. and Schetz, J. A., "Effects of Swirl and High Turbulence on a Jet in a Crossflow," *Journal of Aircraft,* Vol. 26, June 1989, pp. 539-546.

[24]Marchman, J. F. III, *Wind Tunnel Lab Manual,* Aerospace and Ocean Engineering Dept., Virginia Polytechnic Inst. and State Univ., Blacksburg, VA, 1983.

[25]Sung. B., "Analysis of the Vortical Flows Around a 60-Deg Delta Wing with Vortex Flaps," Ph. D. Dissertation, Virginia Polytechnic Inst. and State Univ., Blacksburg, VA, 1985.

[26]*General Purpose Contouring Program User's Manual,* California Computer Products, Inc., Anaheim, California, April 1971.